Congresso de Métodos Numéricos em Engenharia 2015
Lisboa, 29 de Junho a 2 de Julho, 2015

VGCM2D-FLEXIBLE: A GENERALIZED PARTICLE CONTACT MODEL FOR ROCK FRACTURE TAKING INTO ACCOUNT PARTICLE DEFORMABILITY

N. Monteiro Azevedo[1]*, M. L. Braga Farinha[1] and M. Candeias[2]

1: Concrete Dams Department
Laboratório Nacional de Engenharia Civil (LNEC)
Av. do Brasil 101, 1700-066 Lisboa, Portugal
e-mail: {nazevedo, lbraga}@lnec.pt, web page: http://www.lnec.pt/organizacao/dbb

2: *Concrete Dams Department*
Laboratório Nacional de Engenharia Civil (LNEC)
Av. do Brasil 101, 1700-066 Lisboa, Portugal
e-mail: marilinecandeias@gmail.com, web page: http://www.lnec.pt/organizacao/dbb

Keywords: Fracture, Rock, Particle modelling, Deformability

Abstract *Rigid particle models taking directly into consideration the physical mechanisms and the influence of the material grain structure have been developed for fracture studies of quasi-brittle material such as rock. A 2D rigid particle generalized contact model (VGCM2D) has been recently proposed which properly reproduces the rock friction angle and the rock tensile strength to compressive strength ratio, while keeping the simplicity and the reduced computational costs characteristic of circular particle models. In this work the VGCM2D contact model is extended in order to include the particle deformability by considering in each particle an inner finite element mesh triangular discretization. The VGCM2D flexible contact model is tested against known experimental data on a granite rock, namely uniaxial and biaxial tests and Brazilian tests. The study carried out shows the importance of considering the particle deformability in order to obtain results closer to the experimental data.*

1. INTRODUCTION

Detailed rigid particle models have been introduced in the study of fracture of continuous media such as concrete and rock in the early 1990s [1-4]. Particle models are conceptually simpler than a continuum approach, and the development of cracks and rupture surfaces appears naturally as part of the simulation process given its discrete nature [5]. The choice of parameters of the interaction laws requires some previous calibration through elementary testing.

The bonded particle model (BPM), as presented in [6], does not match the ratio of the compressive strength to tensile strength that occurs in rock. In addition, the macroscopic friction angle obtained with this model in triaxial testing is much lower than the known hard rock experimental values. A 3D spherical particle model has recently been proposed that gives a good agreement with the triaxial failure envelope obtained in Lac du Bonnet granite rock by including a frictional term for the contact shear strength and by increasing the number of contacts per particle [7]. In [8] a 3D particle model is proposed that by allowing moment transmission at the contact level and by using a Delaunay 3D edge criteria for particle interaction is able to predict not only the failure envelopes but also the compressive to tensile strength ratio of a hard rock such as Lac du Bonnet granite.

Due to the high computational costs associated with 3D particle models, 2D models are still being developed and adopted for rock fracture studies. Several enhancements have been proposed in 2D particle models, namely to use a clumped particle logic [9] or to adopt a polygonal grain structure [10,11]. A 2D rigid particle generalized contact model (VGCM2D-Rigid) has been recently proposed [12]. The latter contact model is shown to properly reproduce the rock friction angle, the rock tensile strength to compressive strength ratio and the rock direct tensile to indirect tensile ratio, while keeping the simplicity and the reduced computational costs characteristic of circular particle models. In the VGCM2D-Rigid contact model a particle generation algorithm is adopted which generates polygonal shaped particles based on the Laguerre Voronois diagrams of the circular particle gravity centres. A polygonal particle model is then approximated by circular particles that interact with each other through a multiple local contact scheme, being the contact height and the contact location given by the common inter-particle Laguerre Voronoi edge.

The performance of the particle models in 2D and 3D needs to be further improved, especially in 3D, where rigid spherical particle models predicts in uniaxial compression a too brittle response with two distinct slopes in the pre-peak region [8]. In the study presented here the VGCM2D-Rigid contact model is further extended in order to include the particle deformability, this is done by considering an inner finite element triangular mesh in each polygonal shaped particle (VGCM2D-Flexible).

In order to keep the model as simple as possible, the contact between the polygonal shaped particles is still handled as if the geometry is in fact circular and the particles are rigid. Like in the rigid version of the model presented in [12] the contact is still located at the corresponding Laguerre Voronoi edge. A scheme is then devised in order to transfer the contact forces from the contact locations to the corresponding nodal points, of the finite element mesh that represents the polygonal shaped particle, and also to properly define the contact relative velocities given the nodal velocities. The particles are considered to be rigidly associated to the inner nodal point of each cell that is initially located at the particle centre of gravity.

The VGCM2D-Flexible contact model is tested against known experimental data on Augig granite rock, namely biaxial tests and Brazilian tests. The results are also compared with those obtained with the VGCM2D-Rigid contact with similar contact properties. The analysis carried out shows the importance of considering the particle deformability in order to obtain results closer to the experimental data.

2. FORMULATION

2.1. Fundamentals

In the DEM, the domain is represented by an assembly of discrete entities that interact with each other through contact points or contact interfaces. The ability to include finite displacements and rotations, including complete detachment, and to recognize new contacts as the calculation progresses are essential features.

The forces acting on each entity are related to the relative displacements of each entity with respect to its neighbours (contacts) and to the entity deformation given its loads. At each step, given the applied forces, Newton's second law of motion is invoked to obtain the new nodal points/particle positions. For a given nodal point/particle the equations of motion, including local non-viscous damping, may be expressed as:

$$F_i(t) + F_i^d(t) = m\ \ddot{x}_i \tag{1}$$

$$M_3(t) + M_3^d(t) = I\ \dot{\omega}_3 \tag{2}$$

where: $F_i(t)$ and $M_3(t)$ are, respectively, the total applied force and moment at time t including the exterior contact contribution, m and I are, respectively, the nodal point/particle mass and moment of inertia, $\ddot{x}_i$ is the nodal point/particle acceleration, $\dot{\omega}_3$ is the nodal point/particle angular acceleration. The damping forces using local non-viscous damping formulation are given by:

$$F_i^d(t) = -\alpha \left|F_i(t)\right| sign(\dot{x}_i) \tag{3}$$

$$M_3^d(t) = -\alpha \left|M_3(t)\right| sign(\omega_3) \tag{4}$$

where, $\dot{x}_i$ is the nodal point/particle velocity, ω_3 the nodal point/particle angular velocity, α the local non-viscous damping and the function $sign(x)$ is given by:

$$sign(x) = \begin{cases} +1\,, & x > 0 \\ -1\,, & x < 0 \\ 0\,, & x = 0 \end{cases} \tag{5}$$

The nodal point forces applied at a given instant of time is defined by three parts:

$$F_i\ (t) = F_i^e(t) + F_i^c(t) + F_i^1(t) \tag{6}$$

where, $F_i^e(t)$ are the external forces applied at the nodal point, $F_i^c(t)$ are the external forces due to the contact interaction with neighbouring entities which only occurs at nodal

points located at the polygonal particle outer boundaries, and $F_i^1(t)$ are the internal forces due to the deformation of the associated triangular plane finite elements adopted in the discretization of each particle [13]. The external forces due to contact interaction are defined in the following section.
As previously mentioned, the particles are considered to be rigidly associated to the inner nodal point of each polygonal particle that is initially located at its centre of gravity.

2.2. VGCM2D-Flexible contact model

The 2D Voronoi generalized flexible contact model (VGCM2D-Flexible) is based on the 2D Voronoi generalized rigid contact model proposed in [12]. The VGCM2D-Flexible contact model includes the particle deformability by considering an inner finite element mesh triangular discretization.
In order to keep the model as simple as possible, the contact between the polygonal shaped particles is handled as if the particle is rigid and its geometry is in fact circular and the contact is located at the corresponding Laguerre Voronoi edge like in the VGCM2D-Rigid contact model [12].
The inner finite element triangular mesh of each Laguerre cell is defined by a Delaunay triangulation of the Laguerre vertexes and the point corresponding to the particle centre of gravity (Figure 1). The VGCM2D-Flexible contact is adopted following the contact geometry of the Voronoi tessellation. The particles are still circular but are considered to interact with neighbouring particles through the polygonal interface edges. Figures 1 a) and 4 d).
In the VGCM2D-Flexible contact model, like in the VGCM2D-Rigid contact model, the contact width and the contact location are defined by the Voronoi tessellation, Figure 1 a). Like in the VGCM2D-Rigid contact model, the contact width corresponds to the length of the associated Voronoi cell edge and the contact location is also defined by the Voronoi cell edge. The VGCM2D-Flexible further requires the definition of the triangular finite elements associated with each Voronoi cell edge (Figure 1). Also the motion of each circular particle, representing the outer geometry of the Laguerre Voronoi cell, is rigidly associated to the inner nodal point that is initially located at the particle centre of gravity.
In the VGCM2D-Flexible contact model, the contact unit normal, n_i, is defined given the particles centre of gravity and the inter-particle distance, d, Fig. 1 b):

$$n_i = \frac{x_i^{[B]} - x_i^{[A]}}{d} \tag{7}$$

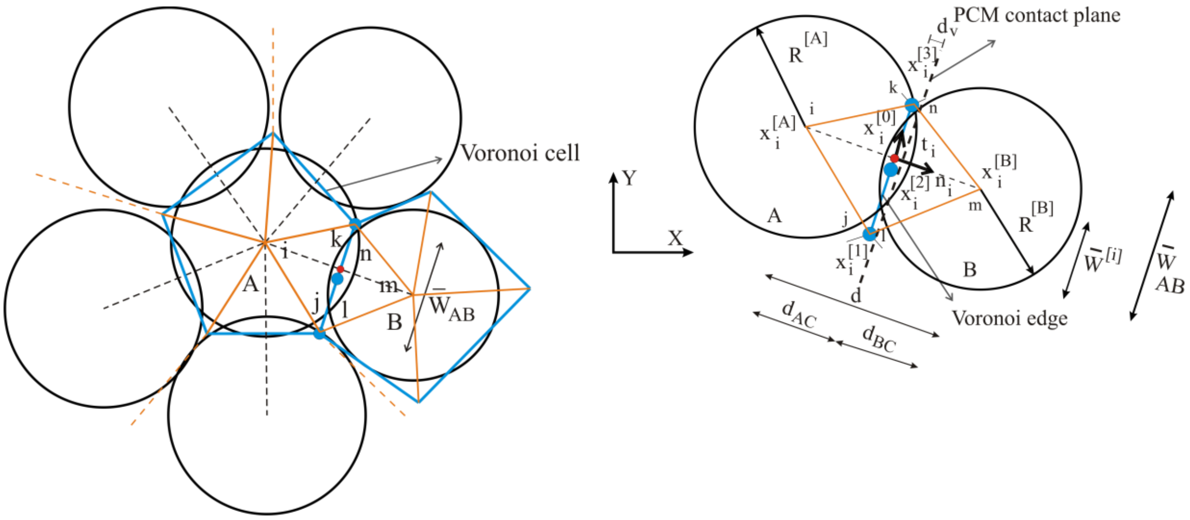

a) Contact width and location at the Voronoi cell b) 3 local contact point scheme

Figure 1.VGCM2D-Flexible contact model for a discretization with 3 local contact points.

In the VGCM2D-Flexible contact model, the contact overlap for the reference contact point, U^n, is defined by:

$$U^n = R^{[A]} + R^{[B]} - d \tag{8}$$

In the VGCM2D-Flexible contact model, the reference contact point, $x_i^{[0]}$, is defined at the associated Voronoi cell edge by:

$$x_i^{[0]} = x_i^{[A]} + \left(R^{[A]} - \frac{1}{2} U^n - d_v \right) n_i \tag{9}$$

where, d_v is the distance along the contact normal between the PCM geometric contact plane of the two circular particles in contact and the adopted contact plane as defined by the corresponding Voronoi cell edge. If the Voronoi cell edge is located along the PCM contact plane ($d_v = 0$) the reference contact point location matches the contact location as defined in the traditional PCM contact model.

The position of each local contact point, $x_i^{[J]}$, is defined relatively to the reference local contact point, using the tangent vector to the Voronoi edge contact plane, $t_i^{[J]}$, and the contact distance in the tangent direction to the reference contact point, $\bar{W}^{[J]}$:

$$x_i^{[J]} = x_i^{[0]} + \bar{W}^{[J]} t_i^{[J]} \tag{10}$$

For the case of a 3 local contact point scheme as defined in Figure 1, the local contact point global coordinates are initially given by the Voronoi tessellation (the mid-point local contact location is given by averaging the Voronoi cell edge end point coordinates). The value of $\overline{W}^{[J]}$ for each local contact point is then defined using equation 10. The same procedure is adopted for other types of local contact point distributions.
The contact forces that are acting on each local contact point, $x_i^{[J]}$, can be decomposed into their normal and shear components with respect to the contact plane:

$$F_i^{[J]} = F_i^{[n,J]} + F_i^{[s,J]} \tag{11}$$

The contact velocity of a given local contact point, which is the velocity of particle B relative to particle A, at the contact location is given by:

$$\begin{aligned} \dot{x}_i^{[J]} &= \left(\dot{x}_i^{[J]} \right)_B - \left(\dot{x}_i^{[J]} \right)_A \\ &= \left(N_{m.\Delta mnl} \dot{x}_i^{[m.\Delta mnl]} + N_{n.\Delta mnl} \dot{x}_i^{[n.\Delta mnl]} + N_{l.\Delta mnl} \dot{x}_i^{[l.\Delta mnl]} \right)_B - \\ &\quad \left(N_{i.\Delta ijk} \dot{x}_i^{[i.\Delta ijk]} + N_{j.\Delta ijk} \dot{x}_i^{[j.\Delta ijk]} + N_{k.\Delta ijk} \dot{x}_i^{[k.\Delta ijk]} \right)_A \end{aligned} \tag{12}$$

where, $N_{m.\Delta mnl}$ is the shape function value associated to nodal point "m" of the corresponding triangular finite element, Δ_{mnl}, at the local contact point location $\dot{x}_i^{[J]}$, and $\dot{x}_i^{[m.\Delta mnl]}$ is the velocity of nodal point "m" of the corresponding triangular plane finite element, see Figure 1 b).
The triangular shape functions values are defined in the traditional way according to the associated triangular areas (positive value clockwise), see Figure 2:

$$\begin{aligned} N_{i.\Delta ijk} &= Area_{\Delta\, jkx^{[J]}} \big/ Area_{\Delta\, ijk} \\ N_{j.\Delta ijk} &= Area_{\Delta\, kix^{[J]}} \big/ Area_{\Delta\, ijk} \\ N_{k.\Delta ijk} &= Area_{\Delta\, ijx^{[J]}} \big/ Area_{\Delta\, ijk} \end{aligned} \tag{13}$$

The contact displacement normal increment, $\Delta x^{[J,N]}$, stored as a scalar, and the contact displacement shear increment, $\Delta x_i^{[J,S]}$, stored as a vector, are given by:

$$\Delta x^{[J,N]} = \left(\dot{x}_i^{[J]} \Delta t \right) n_i \tag{14}$$

$$\Delta x_i^{[J,S]} = \left(\dot{x}_i^{[J]} \Delta t \right) - \Delta x^{[J,N]} n_i \tag{15}$$

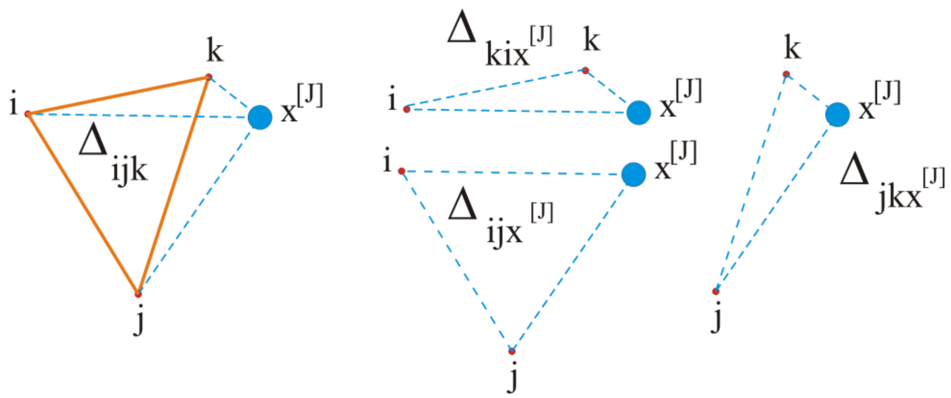

Figure 2.VGCM2D-Flexible contact model triangular shape functions at local contact point $x_i^{[J]}$.

The local contact point overlap, $U^{J,n}$, is defined incrementally for all the local points based on the current contact velocity timestep, Δt:

$$U^{J,n} = U^{J,n\,old} + \left(\dot{x}_i^{[J]}\, n_i \right) \Delta t \tag{16}$$

Given the normal and shear stiffnesses of the local contact point, the normal and shear forces increments are obtained following an incremental linear law:

$$\Delta F_i^{[J,N]} = -k_n^J \; \Delta x_i^{[J,N]} \tag{17}$$

$$\Delta F_i^{[J,S]} = -k_s^J \; \Delta x_i^{[J,S]} \tag{18}$$

Due to the fact that the shear contact force is stored in global coordinates it is necessary to redefine it in the updated contact plane using:

$$F_i^{[J,S.old]} = F_i^{[J,S.old]} - e_{ij3} e_{3mn} F_j^{[J,S.old]} n_m^{old} n_n \tag{19}$$

The predicted normal and shear forces acting at the local contact point are then updated by applying the following equations:

$$F^{[J,N.new]} = F^{[J,N.old]} + \Delta F^{[J,N]} \tag{20}$$

$$F_i^{[J,S.new]} = F_i^{[J,S.old]} + \Delta F_i^{[J,S]} \tag{21}$$

Given the predicted normal and shear contact forces, the adopted constitutive model is applied. It is necessary to carry out adjustments if the predicted forces do not satisfy the constitutive model, this adjustment is model dependent. The resultant contact force at the local contact point is then given by:

$$F^{[J]} = F^{[J,N]}\, n_i + F_i^{[J,S]} \tag{22}$$

The contact force at each local contact point is then transferred to the nodal points of the associated finite element triangle given the nodal shape functions. For the triangular plane finite element associated with particle *A* and for the triangular element associated with particle *B* (Figure 1b)) the local contact forces are distributed to each nodal point according to:

$$F^c_{i.\Delta ijk} = F^c_{i.\Delta ijk} - F_i^{[C]} N_{i.\Delta ijk} \tag{23}$$

$$F^c_{m.\Delta mnl} = F^c_{m.\Delta mnl} + F_i^{[C]} N_{m.\Delta mnl} \tag{24}$$

The VGCM2D-Flexible contact model can be transformed into a PCM-Flexible contact model if only one local contact point, located at the reference contact point, is adopted in the contact discretization, and if the distance of the adopted contact plane, located at the Voronoi cell edge, to the PCM contact plane is zero ($d_v = 0$).

The VGCM2D-Flexible contact model naturally incorporates the force versus relative particle displacement relationships of the traditional point contact model (PCM). In addition, it provides both moment transmission and simple physical constitutive models based on standard force displacement relationships. Within a small displacement hypothesis, the VGCM2D-Flexible contact model is very similar to the traditional finite element joint interface model. Under a large displacement hypothesis, the VGCM2D-FLexible contact model approximates the interaction between two polygonal flexible particles by considering that they are both circular and rigid.

2.3. Numerical stability

When only a steady state solution is sought, a mass scaling algorithm is adopted in order to reduce the number of timesteps necessary to reach the desired solution. The nodal points masses are scaled so that the adopted centred-difference algorithm has a higher rate of convergence for a given loading step. The nodal point scaled mass used in the calculations are set assuming a unit time increment, $\Delta t = 1$, given the nodal point associated stiffness at a given time through:

$$m_{scaled} = 0.25\, K_t \tag{25}$$

The latter equation is the result of the application of the Gershgorin's theorem [13] which guarantees that the highest frequency of a structural system is less than or equal to the ratio of the sum of the absolute values of a row of the stiffness matrix and the sum of the mass matrix row. An upper bound of the translation stiffness K_t associated to the GCM2D-Flexible contact model must be found at a given timestep:

$$K_t = \sum_{c=1}^{N} 2\left(\sum_j k_n^J + \sum_j k_s^J\right) N_{i.\Delta ijk} \tag{26}$$

where, $\sum_{c=1}^{N}$ indicates a summation along the "N" contacts associated with nodal point "i", k_n^J and k_s^J are the contact normal and shear stiffnesses, respectively, associated with local point J and $N_{i.\Delta ijk}$ is the shape function associated with nodal point "i" of the triangular plane finite element associated with the VGCM2D-contact.

2.4. Local contact stiffness and strength

The VGCM2D-Flexible contact model requires the user definition of the contact deformability parameters, namely the Young's modulus of the equivalent continuum material ($\bar{E}$) and the constant that relates the normal stiffness and the shear stiffness spring value (η). In this work the local contact normal and shear stiffnesses are given by:

$$k_n^J = K_n A_c^J \tag{27}$$

$$k_s^J = \eta\, k_n^J \tag{28}$$

where, A_c^J is the contact area associated with the local point J and K_n is the normal stiffness adopted for the contact.

The total contact area is given by $A_c = \bar{W}\, t$, where $\bar{W}$ is the contact interface width given by the Voronoi cell edge length and t is the out of plane thickness. In the study presented here, the contact area associated with each local contact point is defined based on a Lobatto quadrature rule [12]. If the local contact point areas and contact locations are defined using a Lobatto quadrature rule higher than 2 local points, the contact rotational stiffness of the VGCM2D flexible contact matches the rotational stiffness of a set of elastic springs uniformly distributed over a rectangular cross-section (width $\bar{W}$ and out of plane thickness t) lying on the contact plane and centred at the reference local contact point, which corresponds to the rotational stiffness value of the PB contact model [6].

The 3 local contact point scheme adopted in Figure 1 follows the Lobatto quadrature rule positioning: two local contact points at each edge end-point and one local contact point in the middle of the segment. The end-points have an associated local contact area of $A_c/6$ and the mid-point has an associated contact area of $2A_c/3$. For the local inter-particle contacts, the VGCM2D-Flexible contact model also requires the definition of the contact strength properties, the maximum contact tensile stress, $\sigma_{n.t}$, the maximum contact cohesion stress, τ, and the contact frictional term, μ_c . The maximum contact local tensile strength, $F^J_{n.\max}$, and the maximum local contact shear strength, $F^J_{s.\max}$, are defined given the user-specified contact strength properties and the current local contact normal force, F^J_n , as follows:

$$F^J_{n.\max} = \sigma_{n.t}\ A^J_c \tag{29}$$

$$F^J_{s.\max} = \tau\ A^J_c + F^J_n\ \mu_c = C^J_{\max} + F^J_n\ \mu_c \tag{30}$$

where $C^J_{\max}$ is the adopted maximum local contact cohesion strength. Figure 3 shows the bilinear softening contact model under tension and shear. The bilinear contact model requires the definition of the contact tensile fracture energy, $G_{f.n}$, and of the contact shear fracture energy, $G_{f.s}$. As soon as the local maximum strength is reached, the local maximum normal tensile and the local maximum cohesion values are reduced based on the current contact damage value, which varies from 0, in the undamaged state, to 1, in a fully damaged state.

The tensile damage value is defined based on the current local contact normal displacement ($D^J_n\left(U^J_n\right)$) Figure 3 a), and the cohesion damage value is defined based on the current local contact shear displacement ($D^J_s\left(U^J_s\right)$), only the cohesion part is affected, Figure 3 b). Figure 3 b) also shows the evolution of the local contact shear strength for a constant value of local contact normal force (F^J_n). In each local contact point the contact damage, D^J_c , is given by the sum of the tensile and shear contact damages. Given the current local contact damage, the local maximum tensile strength and maximum local cohesion strength are updated to:

$$F^{J.Current}_{n.\max} = D^J_c\ F^J_{n.\max} \tag{31}$$

$$C^{J.Current}_{\max} = D^J_c\ C^J_{\max} \tag{32}$$

A local contact crack is considered to occur when the maximum possible damage ($D^J_c = 1$) is reached. At this stage the local contact point is only considered to work under pure friction. A local contact crack is considered to be a tensile crack if the local contact was under a shear/tensile loading state when the maximum damage was reached. A local contact crack is considered to be a shear crack if the local contact was under a shear/compression loading state when the maximum damage was reached.

If the adopted contact fracture energy is equal to the energy corresponding to the elastic behaviour, the response of the bilinear model is the same as the response obtained using a traditional brittle Mohr-Coulomb model with tension cut-off. By using a bilinear softening model at the contact level the fracture propagation occurs in a smoother and more controlled way than the numerically observed with a brittle model, allowing a less brittle response. In [12] it is shown that a bilinear softening contact model predicts a direct tensile strength to indirect tensile strength ratio closer to that expected in rock, which is not possible to obtain with a brittle contact law.

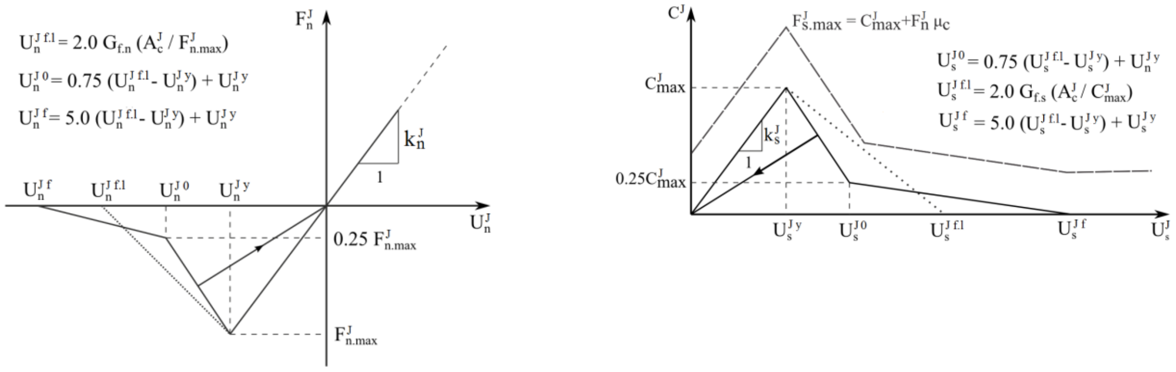

a) Normal direction

b) Shear direction

Figure 3. Bilinear softening constitutive laws under tension and shear.

2.5. Model generation

In [12] a particle generation scheme was proposed which generates polygonal shaped particles based on the Laguerre Voronois using a weighted Delaunay triangulation of the circular particle gravity centres. A Laguerre tessellation is preferred because it generates Voronois with edges closer to the PCM geometric contact planes when considering two particles in contact. A traditional Voronoi tessellation based on a simple Delaunay triangulation generates Voronois with edges closer to the mid-distance between the particles centre of gravity, which for particles of different sizes may lead to Voronoi edges too far away from the PCM contact planes.

The initial circular particle assembly is created by first inserting the particles with half their radius ensuring that the particles do not overlap with each other. Then the particle real radius is adopted and a DEM cohesionless type solution is obtained, leading to a redistribution of the particle overlap throughout the assembly, Figure 4 a). The particle centres of gravity are then triangulated using a weighted Delaunay scheme, Figure 4 b), and then the polygonal shaped particles are obtained given the Laguerre tessellation based on the weighted Delaunay triangulation.

In each polygonal shape particle (Laguerre cell) nodal points are created at the Laguerre cell vertexes and at the particle centre of gravity. A Delaunay triangulation of the nodal points of each Laguerre cell is performed, Figure 4 c). Finally, the VGCM2D-Flexible contact is adopted following the contact geometry of the Voronoi tessellation. The particles are still circular but are considered to interact with the neighbouring particles through the polygonal interface edges, Figure 4 d). Each circular particle is considered to be rigidly associated to the inner nodal point initially located at the particle centre of gravity.

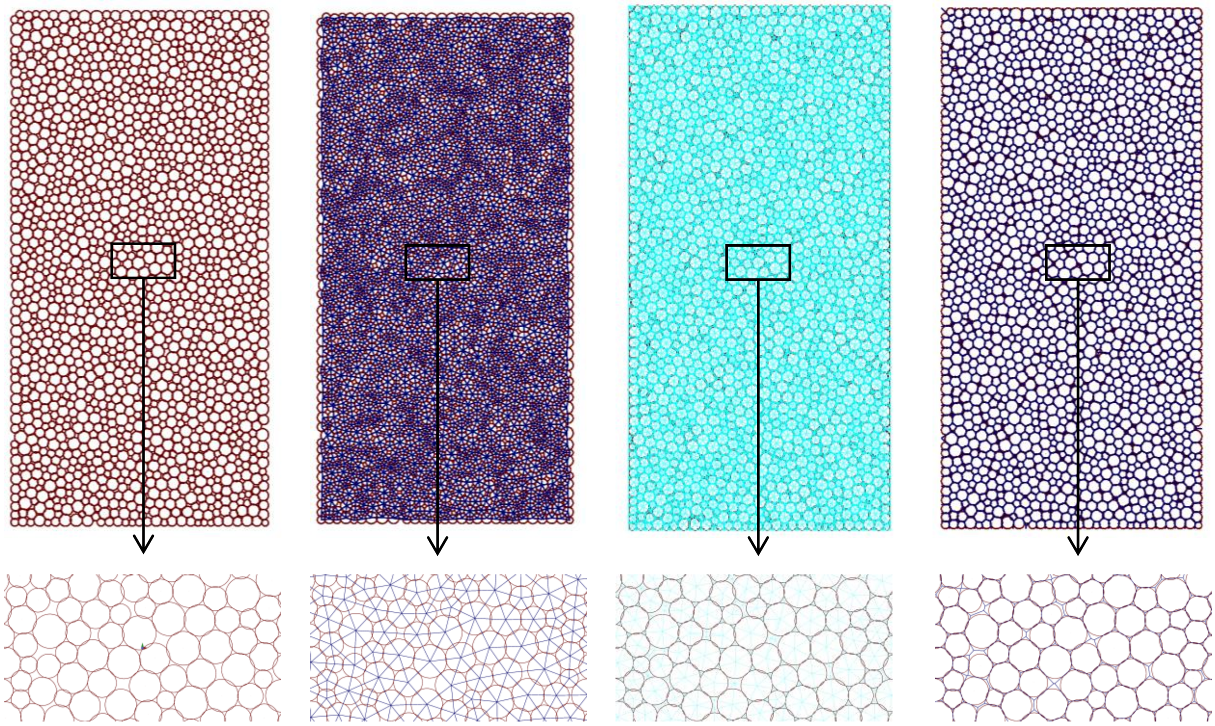

Figure 4. From the grain structure to the VGCM2D-Flexible contact including plane element mesh.

The particle generation scheme properties are the maximum particle diameter, D_{max}, the minimum particle diameter, D_{min}, the radius distribution, the porosity, n, and the particles density, ρ. In the simulations that were carried out, a porosity value of 10% was adopted in the definition of the initial number of particles to be inserted [6]. The adopted porosity is not associated with the porosity of the rock to be modelled. From Figures 4 c) and 4d) it can be verified that the adopted scheme generates a compact flexible particle assembly with polygonal edge interactions that has no porosity.

2.6. Model parameters

The VGCM2D-Flexible model requires the definition of seven elastic and strength parameters associated to the contacts. It is also requires the definition of the Young modulus and the Poisson's coefficient of the triangular finite elements that are adopted in the inner discretization of each Laguerre cell. The elastic response of the particle assembly is related with the elastic contact properties, Young's modulus of the equivalent continuum material, $\overline{E}$ and the constant that relates the normal and the shear stiffness spring value (η), and with the continuum elastic properties adopted in the finite element mesh.

The strength macroscopic response requires the definition of the maximum contact tensile stress, $\sigma_{n.t}$, the maximum contact cohesion stress, τ, the frictional term, μ_c , and both the contact tensile, $G_{f.n}$, and the contact shear, $G_{f.s}$, fracture energies. In the finite element mesh an elastic behaviour is adopted.
The properties associated with the particle generation can also be understood as model parameters, namely the grain size distribution given by the maximum diameter (D_{max}) and the minimum diameter (D_{min}) of the circular particle assembly. The particle distribution adopted should be as close as possible to the grain size distribution of the rock to be studied.
Given that a direct relationship between micro-properties and macro-properties is difficult to establish, the micro-properties are traditionally defined through a calibration process in order to reproduce the known macroscopic material behaviour.

3. BIAXIAL AND BRAZILIAN TESTS IN A GRANITE ROCK

3.1. Numerical setup

The proposed VGCM2D-Flexible contact model is validated against known uniaxial, biaxial and Brazilian tests in a granite rock (Augig) [11]. The uniaxial tests, without lateral confinement pressure, and the biaxial tests with lateral confinement pressure are performed in samples with 80 mm x 160 mm. The Brazilian tests are performed on circles with a diameter of 80 mm. The simulations are performed in two dimensions, therefore the particle assembly is considered to have 80 mm thickness. The course aggregate of Augig granite ranges from 2.0 to 6.0 mm [11]. In order to simulate this rock, both geometries where discretized with particles with a uniform diameter distribution ranging from 2.0 to 4.0 mm. The uniaxial tests and the biaxial tests with lateral confinement have in average 1630 particles, Figures 5 a) and 5 b), the Brazilian tests have in average 640 particles, Figure 5 c).
Figure 5 also shows the particle radius with a 50% reduction in order for the adopted inner triangular plane element mesh to be visible. In the biaxial tests the plane element triangular mesh that is adopted, in order to model the particle deformability, has an average number of 11000 nodal points and 9500 triangular finite elements. In the Brazilian tests the inner plane finite element mesh, which allows particle deformability, has in average 4300 nodal points and 3600 triangular finite elements. For the triangular finite elements a plane stress condition was adopted.
As mentioned, within the VGCM2D-Flexible contact model, the particles are only required in order to set the contact geometry, the remaining calculations are performed taking into account the nodal points. The particles are considered to be rigidly associated to the nodal points that are initially created at the particle gravity centres. In the biaxial tests where a confinement pressure is considered, the initial isotropic pressure is applied through both the upper plate and the lateral boundaries by applying the desired pressure at the corresponding finite element edges. The finite element nodal points at the upper and at the lower plate have their motion restrained in the vertical direction, a zero value at the lower plate and the imposed value at the upper plate.

In the biaxial tests with confinement, after setting the isotropic confinement stress, the nodal points at the upper wall have their motion in the vertical direction given by a small downward velocity of 6.25×10^{-7} m/s, in order to simulate quasi-static conditions. In the uniaxial compression test the same value of downward velocity is adopted for the nodal points at the upper plate from the beginning of the simulation, and in the uniaxial direct tensile test the same value of velocity is adopted for the nodal points at upper plate but now in the upward direction.

In the Brazilian tests the quasi-static load is applied by giving a downward velocity, 6.25×10^{-7} m/s, to the upper plate rigid block which interacts with the neighbouring particles through a PCM-Flexible contact model that follows the principles here described for the GCM2D-Flexible contact model adopting only a single contact point. The lower plate rigid block has its motion restrained. In all tests a local damping coefficient of 0.7 is adopted. The quasi-static plate velocity values are computed so that the measured macro-properties are not altered if the velocity value is further reduced.

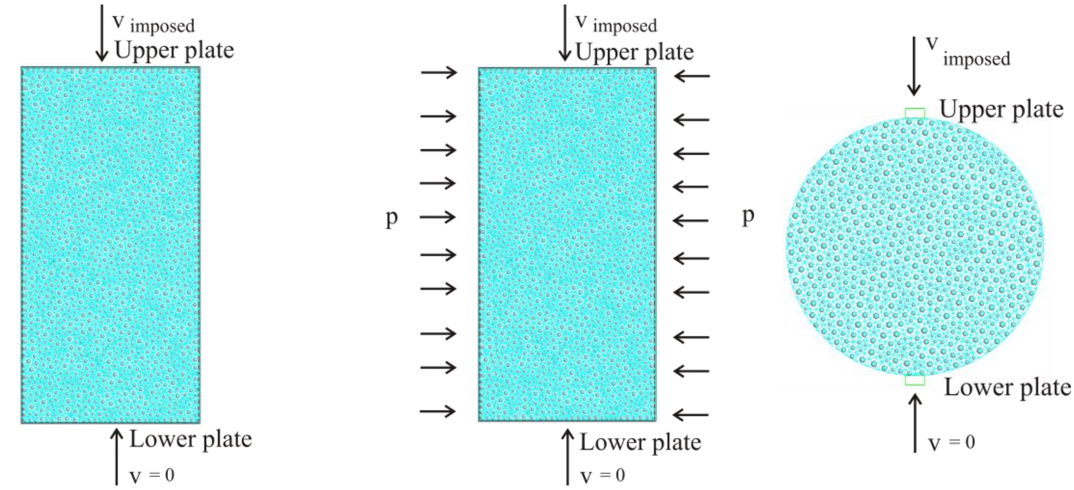

Figure 5. Boundary conditions adopted in the VGCM2D-Flexible numerical simulations

Table 1 presents the micromechanical elastic and strength properties that were adopted for the VGCM2D-Flexible contact model, for brittle and bilinear softening contact laws. The strength values are the same as the values adopted in the VGCM2D-Rigid contact model [12,15] that were found to predict numerical results closer to the experimental data of a Augig granite rock [11].

For the finite element plane mesh, a plane stress condition with a young modulus of 51.6 GPa and a Poisson's coefficient of 0.23 was adopted. In the VGCM2D-Rigid contact model [12,15] the same value of the constant (η) that relates the normal to shear local contact stiffness was adopted, and an approximated value of 109.83×10^{8} kPa/m was adopted for the normal stiffness of the VGCM2D-Rigid contacts.

	K_n [kPa/m]	η	μ_c	$\sigma_{n.t}$ [MPa]	τ [MPa]	$G_{f,n}$ [N/m]	$G_{f,s}$ [N/m]
VGCM2D-Flexible-Brittle	211.56x10^8	0.285	0.40	13.7	48.8	-	-
VGCM2D-Flexible-Bilinear	211.56x10^8	0.285	0.50	11.5	33.25	66.1	2078.7

Table 1. Elastic and strength micro-properties adopted in VGCM2D-Flexible contact model.

3.2 Deformability

Several parametric studies were carried in order to assess the influence of the contact elastic parameters and of the elastic parameters adopted in the finite element mesh in the macroscopic particle assembly elastic response, given by its Young's modulus (E) and Poisson's coefficient (υ). Note that the local contact normal stiffness is proportional to the contact elastic parameter (K_n) and that the local contact shear stiffness is related to the normal contact stiffness through the elastic parameter η. For the VGCM2D-Flexible contact the Young's modulus and the Poisson's coefficient of the plane element mesh were kept constant.

Figure 6 a) shows that in the VGCM2D-Rigid contact model both contact elastic parameters influence the macroscopic Young's modulus of the particle assembly, being the latter elastic macroscopic constant more sensitive to the shear to normal stiffness ratio for higher K_n values. Figure 6 b) shows that in the VGCM2D-Rigid contact model the macroscopic Poisson's coefficient is mainly influenced by the shear to normal stiffness relationship (η).

Figures 6c) and 6d) show for the VGCM2D-Flexible contact model the macroscopic elastic response variation. In both figures the dashed line represents the corresponding elastic values adopted for the finite element plane elements. It can be seen that for the VGCM2D-Flexible contact model the contact elastic parameters, the parameter η that represents the normal to shear contact stiffness ratio and the normal contact stiffness, has a lesser effect than in the rigid contact model.

In 3D it is known that a very low value of η is required in order to match the elastic response [12]. A reduced value of η (lower than 0.1) predicts two distinct slopes before the pre-peak is reached in the uniaxial compression tests. In the 2D simulations here carried it can be seen that the rigid contact model for a value of η equal to 0.285 predicts two slightly different slopes in the stress-strain axial response under uniaxial compression before the peak response is reached (Figure 9a).

The fact that the VGCM2D-Flexible contact model response is less influenced by the coefficient η is a clear indication that a better response can be obtained in 3D with a VGCM3D-Flexible contact model. Figure 7 shows the macroscopic elastic response for a variation of the η coefficient for different values of the Poisson's coefficient adopted in the inner finite element mesh (0.15, 0.23 and 0.35). By varying the latter parameter it is possible to obtain different values for the macroscopic Poisson's ratio for the same elastic contact parameters. Figure 7a) also shows that the macroscopic Young's modulus is not influenced by the Poisson's ratio adopted in the finite element mesh.

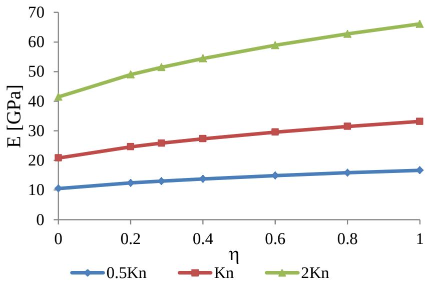

a) VGCM2D-Rigid contact model: Macroscopic Young's modulus for varying η

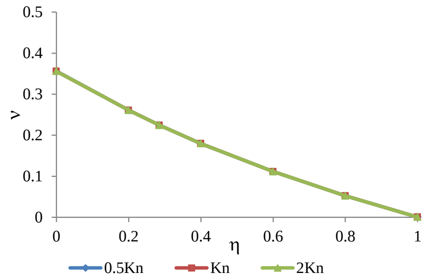

b) VGCM2D-Rigid contact model: Macroscopic Poisson's coefficient for varying η

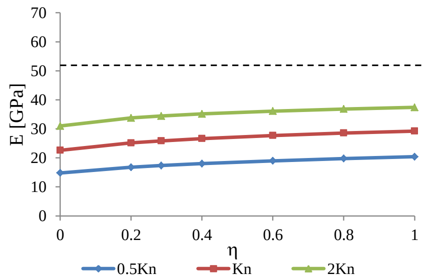

c) VGCM2D-Flexible contact model: Macroscopic Young's modulus for varying η

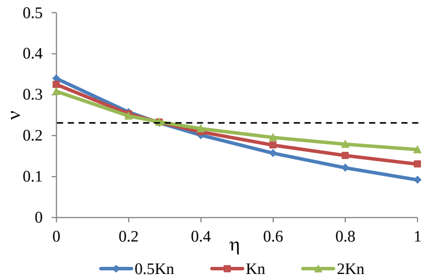

d) VGCM2D-Flexible contact model: Macroscopic Poisson's coefficient for varying η

Figure 6. Influence of the contact deformability parameters (K_n and η) on the elastic macroscopic properties of the particle assembly (E and υ) for the VGCM2D-Rigid contact model [12] and VGCM2D-Flexible contact model.

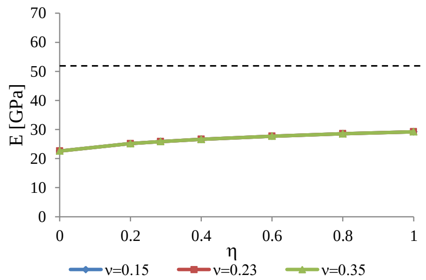

a) VGCM2D-Flexible contact model: Macroscopic Young's modulus for varying η

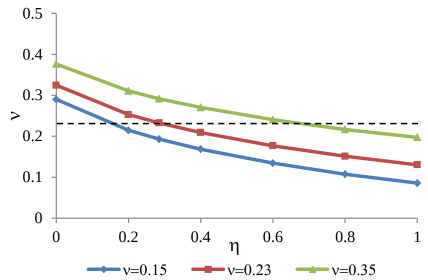

b) VGCM2D-Flexible contact model: Macroscopi Poisson's coefficient for varying η

Figure 7. Influence of the Poisson's coefficient of the inner finite element mesh on the elastic macroscopic properties of the particle assembly (E and υ) for the VGCM2D-Flexible contact model.

3.3 Strength envelope

The Augig granite macro-properties presented in [11] are shown in Table 2, along with the VGCM2D-Flexible calibrated model predictions (brittle and bilinear laws) as well as the response predicted with the VGCM2D-Rigid contact model [12,15] the results of which

were found to be very close to experimental data.
Table 2 shows that both the VGCM2D-Flexible and the VGCM2D-Rigid contact models, after a calibration procedure, are able to predict well the macroscopic response. It can also be seen that the numerical results predicted with the VGCM2D-Flexible contact model with a brittle constitutive law are very close to those obtained with the rigid version. It can also be verified that the VGCM2D-Flexible contact model with a brittle law also predicts an indirect tensile strength lower than the direct tensile strength contrary to the known experimental results. Table 2 also shows that the VGCM2D-Flexible contact model with a bilinear constitutive law predicts, for the same values of contact fracture energy, a higher strength envelope, indicating that, as expected, it is possible to obtain a better agreement with the VGCM2D-Flexible contact model adopting a lower contact fracture energy value. Like in the rigid contact model, the VGCM2D-Flexible contact model requires a bilinear contact softening law in tension and shear in order to predict an indirect tensile strength in the same range or slightly higher than the predicted direct tensile strength.

	E [GPa]	ν	σ_c [MPa]	$\sigma_{t.dir}$ [MPa]	$\sigma_{t.ind}$ [MPa]	c [MPa]	ϕ [°]
Augig granite [11]	25.8	0.23	122.1	-	8.8	21.0	53.0
VGCM2D-Rigid (Brittle)	25.8	0.23	119.4	8.0	5.4	21.5	42.1
VGCM2D-Flexible (Brittle)	25.9	0.23	127.2	8.5	5.9	27.7	43.0
VGCM2D-Rigid (Bilinear)	25.8	0.23	123.4	9.2	11.9	22.4	50.0
VGCM2D-Flexible (Bilinear)	25.9	0.23	140.4	10.1	13.7	23.6	53.0

Table 2. Augig granite macro-properties (Experimental and Numerical).

Figure 8 shows the experimental strength envelopes obtained for Augig granite [11] the Hoek-Brown failure criterion applied to the Augig granite experimental values and the predicted values adopting the VGCM2D-Flexible and the VGCM2D-Rigid contact models following both brittle and bilinear softening contact laws. As previously mentioned it can be seen that the VGCM2D-Flexible contact model with a bilinear softening law requires a lower contact fracture energy when compared with the rigid contact model. It can also be verified that for the brittle law, the consideration of the particle deformability has a little effect on the strength envelope, Figure 8 a).
Figure 9 shows the axial stress-strain response for the VGCM2D-Flexible and the VGCM2D-Rigid contact models, for a brittle contact law and for a bilinear softening contact law. For the case of a brittle contact constitutive law it can be verified that the VGCM2D-Flexible contact model gives a less brittle response. This can be explained by the fact that with a flexible contact model the local contact points inter particle distance at failure is much closer than the local points inter-particle distance at failure with a rigid model, because in the latter the contact normal stiffness is lower as it also needs to represent the overall particle assembly deformability.
For a bilinear softening law both the VGCM2D-Flexible and the VGCM2D-Rigid contact models response have a very sudden drop after the peak value is reached. It is expected

that a VGCM2D-Flexible contact model with lower contact fracture energy will predict a less brittle response because the inter-particle contacts will be closer at contact failure, as the maximum allowable displacement is smaller ($U_n^{J\,f}$ Figure 3a)).

Figure 9 also shows that with a rigid contact model the predicted stress strain response has two distinct slopes for a zero confinement pressure (uniaxial compression). It can be seen that the VGCM2D-Flexible contact model predicts the expected single slope before the peak value is reached. As mentioned before this erroneous behaviour is even clearer in 3D particle models which require a very low coefficient η indicating that the consideration of particle deformability can solve this issue.

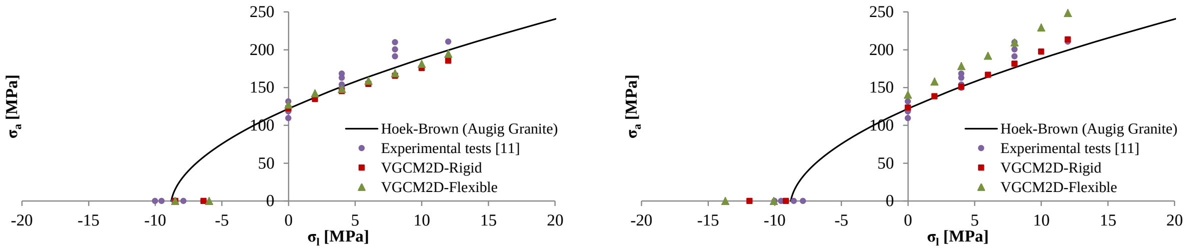

a) Brittle contact constitutive law b) Bilinear softening contact constitutive law

Figure 8. Strength envelope: Hoek-Brown failure criterion; experimental tests [11] and VGCM2D-Rigid and VGCM2D-Flexible contact models.

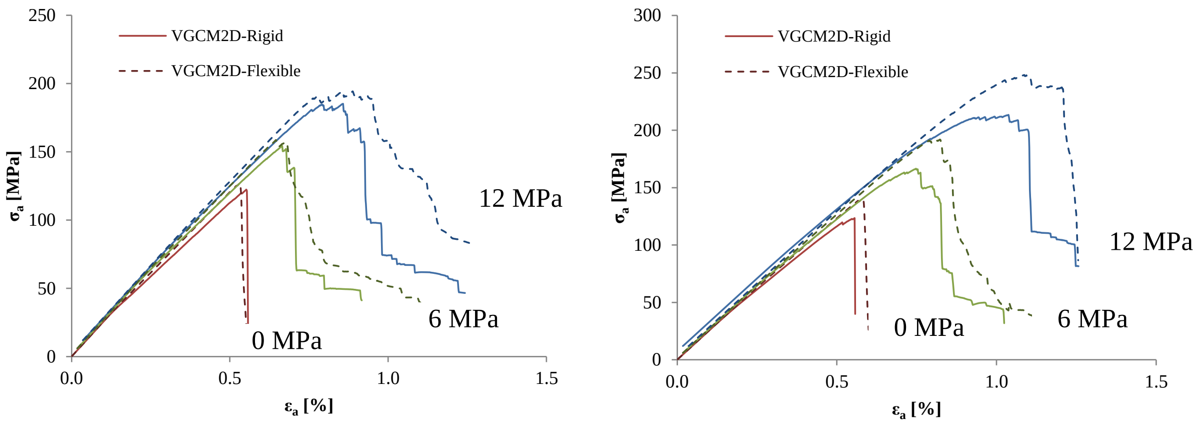

a) Brittle contact constitutive model b) Bilinear softening contact constitutive model

Figure 9. VGCM2D-Flexible (Bilinear) contact model predicted failure patterns

4. CONCLUSIONS

A generalized 2D flexible contact model, VGCM2D-Flexible, which enables moment transmission and contact discretizations with multiple local contact points is presented. The contact width and location are given by the Laguerre Voronois of the particle centre of gravities, and the neighbouring particles are set given the Delaunay triangulation. The particle deformability is included by considering an inner finite element mesh triangular discretization (VGCM2D-Flexible) on each Laguerre Voronoi (polygonal shaped particles).

In order to keep the model as simple as possible, the contact between the polygonal shaped particles is considered as if the particle is rigid and its geometry is in fact circular. The contact is initially located at the corresponding Laguerre Voronoi edge. In the flexible version, the particles gravity centres are considered to be rigidly associated to the inner nodal point of each cell that is initially located at the particle centre of gravity. An explicit formulation of the VGCM2D-Flexible contact model is then presented which shows how the contact forces are transferred from the contact locations to the corresponding nodal points of the finite element mesh that represents the polygonal shaped particle and also how the contact relative velocities are defined given the nodal point velocities. Within a small displacement hypothesis, the VGCM2D-Flexible contact model is very similar to the traditional finite element joint interface model. Under large displacements, the VGCM2D-FLexible contact model approximates the interaction between two polygonal flexible particles by considering that they are circular and rigid.

By including the particle deformability it is possible to obtain a good elastic macroscopic agreement adopting a higher value for the coefficient that relates the normal to shear contact stiffness. It is known that in 3D a very low normal to shear coefficient predicts two distinct slopes before the peak value is reached. This study highlights that even in 2D simulations, where a higher normal to shear stiffness coefficient is adopted, the particle deformability consideration is also important in order to predict a clear single slope before the peak is reached in uniaxial compression.

The presented results show that the VGCM2D-Flexible contact predicts a more ductile response under a brittle constitutive law and it also requires a smaller value of contact fracture energy in order to correspond more closely with the response predicted with the rigid contact version under a bilinear constitutive contact law. The studies also show the need to incorporate a bilinear softening constitutive model at the contact level in order to obtain a better agreement between the direct tensile strength and the indirect tensile strength even when the particle deformability is taken into account. The latter ratio cannot be correctly predicted with a simple brittle model. As shown particle assemblies with bilinear softening contact laws still predict a brittle macroscopic response under tensile, compression and biaxial states of stress. The bilinear contact model, for the level of contact fracture energy adopted, does not significantly change the fracture process; it mainly slows down the rupture evolution and slightly induces a higher localization of the final crack patterns.

The analysis that is carried out shows that by including the particle deformability a more realistic hard rock macroscopic behaviour is predicted even if, for computational reasons, a simplified circular particle interaction is adopted. This effect is expected to be even more relevant in 3D simulations.

REFERENCES

[1] K. Meguro and M. Hakuno, “Fracture analysis of concrete structures by the modified

distinct element method", *Structural Engineering / Earthquake Engineering*,Vol **6**(2), pp. 283-294, (1989).

[2] D. Potyondy and P.A. Cundall, *Modeling rock using bonded assemblies of circular particles*, Aubertin, Hassani, Mitri eds. *2nd North American Rock Mechanics Symposium*, Balkema, pp. 1937-1944, (1996).

[3] E. Schlangen and E. Garboczi, "Fracture simulations of concrete using lattice models: Computational aspects", *Engineering Fracture Mechanics*, Vol **57**(2/3), pp. 319-332, (1997)

[4] J.E. Bolander and S. Saito, "Fracture analyses using spring networks with random geometry", *Engineering Fracture Mechanics*, Vol **61**(5-6), pp. 569-591, (1998).

[5] P. Cundall, "A discontinuous future for numerical modelling in geomechanics?", *Geotechnical Engineering*, Vol **149**(1), pp. 41-47, (2001).

[6] D. Potyondy and P.A. Cundall, "A bonded-particle model for rock", *International Journal of Rock Mechanics and Mining Sciences*, Vol **41**(8), pp. 1329-1364, (2004).

[7] Y. Wang, F. Tonon, "Modeling Lac du Bonnet granite using a discrete element model". *International Journal of Rock Mechanics and Mining Sciences*, Vol **46**(7), pp. 1124-1135, (2009) .

[8] N. Monteiro Azevedo, J. Lemos, "A 3d generalized rigid particle contact model for rock fracture". *Engineering Computations: International Journal for Computer-Aided Engineering and Software*, Vol **30**(2), pp. 277-300, (2013).

[9] N. Cho, C. Martin, and D.C. Sego, "A clumped particle model for rock. *International Journal of Rock Mechanics and Mining Sciences*, Vol **44**, pp. 997-1010, (2010).

[10] D. Potyondy, *A grain based model for rock: approaching the true microstructure*. In: Li C, et al (eds) *Proceedings of Rock Mechanics in the Nordic Countries*, Konsberg: Norwegian group for rock mechanics, pp. 225-234, (2010).

[11] T. Kazerani and J. Zhao, "Micromechanical parameters in bonded particle method for modelling of brittle material failure". *International Journal of Numerical and Analytical Methods in Geomechanics*, Vol **34** (18), pp. 1877-1895, (2010).

[12] N. Monteiro Azevedo, M. Candeias and F. Gouveia, "A Rigid Particle Model for Rock Fracture Following the Voronoi Tessellation of the Grain Structure: Formulation and Validation", *Rock mechanics and Rock Engineering*, Vol **48** (2), pp. 535-557, (2015).

[13] J. V. Lemos and P. Cundall, Earthquake analysis of concrete gravity dams on jointed rock foundations. In *Distinct Element Modelling in Geomechanics*, A.A. Balkema, Rotterdam, pp. 117–143, (1999).

[14] P. Underwood, Dynamic relaxation. In T. Belytschko and T. Hughes (eds) *Computation Methods for Transient Analysis*, North-Holland, New York, pp. 246-265, (1983).

[15] N. Monteiro Azevedo and F. Gouveia, "Um modelo discreto de partículas 2D para simulação da fratura em rocha: Formulação e Calibração", *Geotecnia*, Vol **129**, pp. 73-101, (2013) (in portuguese).